Hindawi
Geofluids
Volume 2022, Article ID 7598831, 12 pages
https://doi.org/10.1155/2022/7598831

*Research Article*

# Study on Energy Distribution Law and Numerical Simulation of Mining Roadway Surrounding Rock

**Guohua Zhang, Chao Ju, Yanwei Duan, Yiwei Wang, Tao Qin, and Chengjia Wu**

*Key Laboratory of Mining Engineering, Heilongjiang Universities, Heilongjiang University of Science and Technology, Harbin 150022, China*

Correspondence should be addressed to Yanwei Duan; 1354070597@qq.com

Received 14 January 2022; Accepted 24 May 2022; Published 23 June 2022

Academic Editor: Zhijie Wen



In underground engineering, the deformation and failure process of the surrounding rock of the roadway is always accompanied by the occurrence of energy. The study of the energy distribution law of the surrounding rock of the roadway plays an important role in its stability. This paper first theoretically analyzes the stress and energy distribution law of the surrounding rock of the roadway, then with the help of numerical simulation method, combined with the existing physical and mechanical parameters, based on the existing support parameters of Dongrong No. 2 Mine, gradually compares and analyzes the distribution of vertical stress and energy under the three support methods of no support, original support, and combined support, and the results found that the vertical stress distribution law under the three support methods is basically the same. High-stress areas appear on the two ribs of the roadway, and low-stress areas appear on the roof and floor. The range of high-stress areas from no support to combined support continues to decrease and becomes more evenly distributed. The energy distribution pattern is basically the same. The overall energy of the coal seam is high. There are high-energy areas at 2 m left and right of the roadway, and the roof and floor energy of the roadway is the smallest. The low energy area extends 5 m up and down, respectively. The range of high-energy areas from no support to combined support is shrinking, and the energy distribution is more uniform.

## 1. Introduction

In underground engineering, the rock mass is in equilibrium before excavation. After excavation, the stress on the surrounding rock of the roadway changes from the original three-way stress state to an approximately two-way stress state, changing the stress environment. In order to achieve a new equilibrium state, part of the energy is transferred to the deep part of the roadway, part is deformed, and part is stored. When the energy storage limit of the rock is reached, the energy is released in the form of deformation and failure. In addition, the occurrence of energy always accompanies the deformation and failure process of the roadway. The practice and theoretical research of roadway support in coal mine indicate that [1–5] the stress of the surrounding rock of the roadway is mainly borne by the surrounding rock itself, and the supporting structure only bears a small part of the stress, but the support plays a crucial role in maintaining the stability of the surrounding rock of the roadway. Moreover, the supporting structure can change the mechanical state of the surrounding rock and absorb part of the energy that causes the deformation and failure of the surrounding rock to reach balance and stability.

At present, a large number of literature from the perspective of energy, supporting theory, and technology conducted in-depth theory research and field application. On the one hand, it mainly focuses on the prevention and treatment of rock burst. Based on the energy balance theory, Gao et al. [6] deduced and analyzed the energy criterion for the

instability of roadway surrounding rock structure under impact disturbance, improved roadway support parameters, and achieved good field results. Based on the energy theory of rock burst, Ju [7] proposed the energy checking design method of rock burst roadway and checked the support system from the perspective of energy. Based on the principle of energy conservation and considering the impact release level, failure characteristics of surrounding rock, and mechanical characteristics of supporting equipment, Wang et al. [8] proposed a method to determine the parameters of three-stage energy-absorbing support. Pan et al. [9] considered that the starting stress condition of rock burst under roadway support was that the stress in the far-field was greater than the critical stress, and the stopping energy condition was that the absorption energy of surrounding rock in the near-field and the absorption energy of support was greater than the release energy in the far-field, and put forward the three-level support theory and technology of roadway rock burst in coal mine.

On the other hand, it focuses on the stability of surrounding rock of mining roadway. For existing projects, Gong et al. [10] conducted similar simulation experiments to study the working principle of NPR anchor cable from the perspective of energy transformation, so as to guide the roadway support design. Shan et al. [11] adopted the energy analysis method to deduce the energy constitutive equation of the yielding anchor bolt and the energy equation under the action of surrounding rock, which were applied to the on-site support and achieved good results. Lin et al. [12] proposed the support scheme with high strength and stable resistance and analyzed the stability of roadway surrounding rock under different support schemes through FLAC$^{3D}$ simulation, so as to determine the reasonable size of reserved coal pillar. Ma et al. [13] studied the control of the surrounding rock in the roof of the roadway with different thicknesses of soft rock formations through UDEC and field monitoring. It is considered that the roadway support scheme is designed based on the energy balance, so that the roadway deformation can be effectively controlled.

The above research provides solid support theory and rich support technology experience from the perspective of energy, but the support research based on energy distribution is relatively insufficient. In this paper, firstly, the stress and energy distribution law of roadway surrounding rock is analyzed theoretically. Then, based on the existing support parameters of Dongrong No. 2 Mine, the stress and energy distribution situation under different support modes is compared and analyzed by numerical simulation, combined with the existing physical and mechanical parameters, and the optimization scheme is proposed. Through on-site verification, the support problem is effectively solved. It provides a solution for similar engineering problems.

## 2. Engineering Background

*2.1. Project Profile.* The average buried depth of the coal seam in the third working face of the 17th layer in the fourth south mining area of Dongrong No. 2 Mine is 450 m, with a coal thickness of 2.80~3.39 m, an average thickness of 3.15 m, and an average dip angle of 17°. The coal seam is stable in deposition, simple in structure, and joints are not developed. The direct roof is fine sandstone with an average thickness of 2.28 m, and the direct floor is siltstone with a thickness of 6.81 m. The roof and floor histogram of coal seam is shown in Figure 1.

*2.2. Support Status and Evaluation.* The ventilation roadway of the third working face of the 17th layer in the fourth south mining area of Dongrong No. 2 Mine is driven along the roof of coal seam, which is supported by "anchor, net, and belt." There are four rows of roof bolts with a row spacing of 1200 mm × 1000 mm and three rows of right rib bolts with a row spacing of 1200 mm × 1000 mm, all using $\Phi$22 mm × 2500 mm type bolts. The roadway adopts trapezoidal section, the net width of the roadway is 4.2 m, the net middle height is 2.65 m, and the sectional area is 11.13m$^2$.

The deformation and failure characteristics of the roadway in Dongrong No. 2 Mine are as follows: the roadway support is difficult, the support cost is high, and the efficiency is low. The roadway will be affected by its special geological and stress conditions such as faults during tunneling. The stress concentration degree in the surrounding rock is large, the roadway convergence is obvious, and the surrounding rock deformation is large. The overlying rock layer on the working face has large overlying strata and fractured zone heights.

The peak values of the working face of abutment pressure are high, and the influence range is also large, which will cause serious disturbance to the stability of the front mining roadway. With the mining of the working face, the structural state and stress state of the roadway continue to change, which further intensifies the difficulty to support.

At present, the existing support design of the roadway is based on the experience data of the adjacent roadway that has been constructed, that is, the engineering analogy method is used for the roadway support design. The overall effect of this supporting method is mediocre, and bolt and metal mesh support is used in some broken areas. Most of the roadway roofs and both ribs have the coal body falling along with the excavation, and the surface of the roadway partially shows the characteristics of irregularity and unevenness. In terms of support conditions, most roadways have different degrees of instability of the roof and two ribs.

## 3. Theoretical Analysis of Roadway Surrounding Rock Energy Distribution

*3.1. Mechanical Model of Roadway Surrounding Rock.* Figure 2 is taken as the mechanical model of the roadway surrounding rock, assuming that the surrounding rock is a homogeneous and isotropic medium, the in situ rock stress is set to $P_0$, and the lateral pressure coefficient is 1. After the roadway is excavated, the surrounding rock is divided into plastic zone, elastic zone, and in situ rock stress zone from the center of the circle. The radius of the plastic zone of surrounding rock is $R_p$, and the radius of roadway is $R_0$. The elastic zone of the surrounding rock is denoted by the superscript "e", and the plastic zone is indicated by the superscript "p."

| Histogram | Lithology | Thickness(m) | Lithologic description |
|---|---|---|---|
| | Siltstone | 4.15 | Dark grey, rich in plant debris, argillaceous cement |
| | Siltstone fine sandstones interbedded | 2.10 | Gray, mainly fine sandstone, siltstone to this end, with wavy horizontal bedding |
| | Coarse sandstone | 10.75 | Grayish white, poor sorting, containing trace gravel, hard cementation |
| | Siltstone | 1.60 | Dark grey, with more fossil plant clasts in abrupt contact with the overburden |
| | 17 coal | 3.15 | Black, block, mainly bright coal, good quality |
| | Siltstone | 3.15 | Dark gray, argillaceous cement, dense, complete core |
| | Fine sandstone | 2.70 | Dark gray, dense, locally containing tuff, solid ratio of significant |
| | Siltstone | 10.60 | Dark gray, argillaceous content increased, with thin layers of coarse sandstone and a small amount of tuff, upper core intact, lower core broken |

Figure 1: Composite strata histogram.

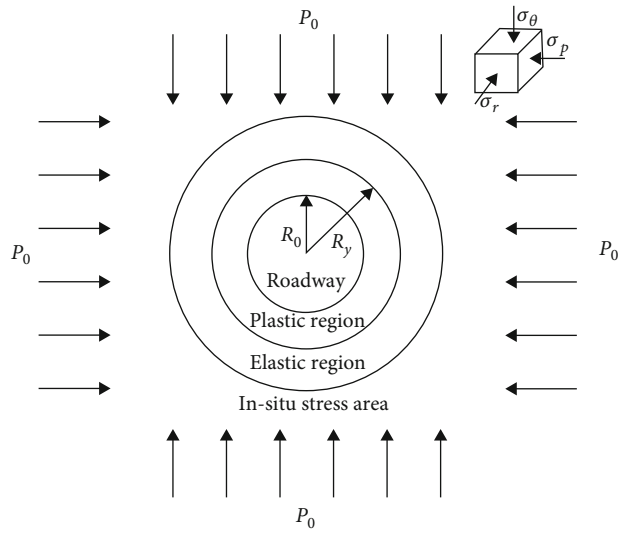


Figure 2: Partition map of roadway surrounding rock.

In order to analyze the mechanical characteristics of the surrounding rock of roadway, the surrounding rock should meet the following conditions [2, 3]:

*3.1.1. Yield Function.*

$$F = \sigma_\theta - \frac{1+\sin\phi}{1-\sin\phi}\phi_r - \frac{2c\sin\phi}{1-\sin\phi} = 0, \quad (1)$$

where $\sigma_\theta$ and $\sigma_r$ are the radial stress and tangential stress of the surrounding rock, respectively; $\varphi$ is the internal friction angle of rock; and $c$ is the cohesion of the rock.

*3.1.2. Differential Equations of Equilibrium.*

$$\frac{d\sigma_r}{dr} + \frac{\sigma_r - \sigma_\theta}{r} = 0, \quad (2)$$

where $r$ is the distance from the research point to the center of the roadway circle.

*3.1.3. Geometric Equations.*

$$\begin{cases} \varepsilon_r = \dfrac{1-\mu^2}{E}\left[(\sigma_r - p_0) - \dfrac{\mu}{1-\mu}(\sigma_\theta - p_0)\right], \\ \varepsilon_\theta = \dfrac{1-\mu^2}{E}\left[(\sigma_\theta - p_0) - \dfrac{\mu}{1-\mu}(\sigma_r - p_0)\right], \end{cases} \quad (3)$$

where $\varepsilon_r$ and $\varepsilon_\theta$ are the radial strain and tangential strain of the surrounding rock, respectively; $\mu$ is the Poisson's ratio of the rock.

Regardless of the elastic displacement caused by in situ rock stress before tunnel excavation, the constitutive

equation is

$$\begin{cases} \varepsilon_r = \dfrac{du}{dr}, \\ \varepsilon_\theta = \dfrac{u}{r}, \end{cases} \tag{4}$$

where $E$ is the elastic modulus of the rock; $u$ is the radial displacement of the surrounding rock.

*3.2. Stress Distribution of Roadway Surrounding Rock.* After the excavation of the roadway, under the condition of supporting reaction force $p_1$, the stress in the elastic zone [2, 3, 14, 15]

$$\begin{cases} \sigma_r^e = p_0 - (c\cos\phi + p_0\sin\phi)\left[\dfrac{(p_0 + c\cot\phi)(1-\sin\phi)}{p_1 + c\cot\phi}\right]^{1-\sin\phi/\sin\phi}\left(\dfrac{R_0}{r}\right)^2, \\ \sigma_\theta^e = p_0 + (c\cos\phi + p_0\sin\phi)\left[\dfrac{(p_0 + c\cot\phi)(1-\sin\phi)}{p_1 + c\cot\phi}\right]^{1-\sin\phi/\sin\phi}\left(\dfrac{R_0}{r}\right)^2. \end{cases} \tag{5}$$

The stress of the plastic zone

$$\begin{cases} \sigma_r^p = (p_1 + c\cot\phi)\left(\dfrac{r}{R_0}\right)^{2\sin\phi/1-\sin\phi} - c\cot\phi, \\ \sigma_\theta^p = (p_1 + c\cot\phi)\left(\dfrac{1+\sin\phi}{\sin\phi}\right)\left(\dfrac{r}{R_0}\right)^{2\sin\phi/1-\sin\phi} - c\cot\phi. \end{cases} \tag{6}$$

The radius of the plastic zone

$$R_p = R_0\left[\frac{(p_0 + c\cot\phi)(1-\sin\phi)}{(p_1 + c\cot\phi)}\right]^{1-\sin\phi/\sin\phi}. \tag{7}$$

Therefore, the stress variation law of the surrounding rock of the roadway in the elastic-plastic state is shown in Figure 3.

*3.3. Energy Distribution of Roadway Surrounding Rock*

*3.3.1. Energy Expression of the Elastic Region.* The elastic strain energy in the surrounding rock of the roadway is a measure of how much work done by internal and external forces in a certain range is stored by the surrounding rock mass. The elastic strain energy density refers to the elastic strain energy per unit volume, which is a function of strain. The following formula is used for calculation [15–17]:

$$v_\varepsilon = \int \varepsilon_i d\sigma_i. \tag{8}$$

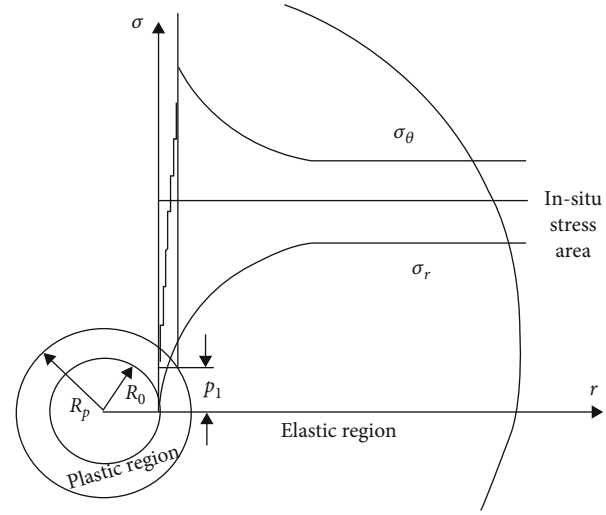


Figure 3: Stress variation law of the surrounding rock of the roadway.

The equations of physics can be expressed as

$$\begin{cases} \varepsilon_1 = \dfrac{[\sigma_1 - \mu(\sigma_2 + \sigma_3)]}{E}, \\ \varepsilon_2 = \dfrac{[\sigma_2 - \mu(\sigma_3 + \sigma_1)]}{E}, \\ \varepsilon_3 = \dfrac{[\sigma_3 - \mu(\sigma_1 + \sigma_2)]}{E}. \end{cases} \tag{9}$$

By substituting Equation (9) into Equation (8), the expression of elastic strain energy density under the elastic state of surrounding rock can be obtained:

$$v_z^e = \frac{\left[\sigma_1^2 + \sigma_2^2 + \sigma_3^2 - 2\mu(\sigma_1\sigma_2 + \sigma_2\sigma_3 + \sigma_1\sigma_3)\right]}{2E}. \tag{10}$$

*3.3.2. Energy Expression of the Plastic Zone.* Using the equal area principle [18–20], the trapezoidal roadway is equivalent to a circular roadway with a radius of 1.88 m. According to Equation (7), the radius of the plastic zone is calculated to be 3.95 m. Combined with the strata histogram, it can be seen that the lithology within this zone is coal seam, siltstone, and coarse sandstone. From the stress-strain curve, the ratio of plastic energy to elastic energy $k$ can be calculated, and the strain energy density in the plastic zone of the surrounding rock of the roadway is

$$v_z^p = kv_z^e. \tag{11}$$

## 4. Numerical Simulation of Roadway Surrounding Rock Stability

*4.1. Establish Model and Select Parameter*

*4.1.1. Selection of Numerical Calculation Software.* FLAC$^{3D}$, as one of the most important numerical analysis software of finite difference method in the field of geotechnical

Table 1: Mechanical parameters and thickness of layers.

| Lithology | Bulk modulus (GPa) | Shear modulus (GPa) | Cohesion force (MPa) | Friction angle (°) | Tensile strength (MPa) | Density (g▪cm$^{-3}$) |
|---|---|---|---|---|---|---|
| Siltstone | 15.6 | 10.8 | 27.25 | 27 | 1.17 | 4.15 |
| Siltstone fine sandstones interbedded | 24.3 | 8.2 | 39.36 | 30 | 4.8 | 2.1 |
| Coarse sandstone | 19.67 | 9.34 | 25.47 | 19 | 10.14 | 10.75 |
| Siltstone | 15.6 | 10.8 | 27.25 | 27 | 1.17 | 1.6 |
| 17 coal seam | 4.24 | 1.11 | 1.51 | 20 | 1.90 | 3.15 |
| Siltstone | 15.6 | 10.8 | 27.25 | 27 | 1.17 | 3.15 |
| Fine sandstone | 20.67 | 10.10 | 43.47 | 19 | 10.14 | 2.7 |
| Siltstone | 15.6 | 10.8 | 27.25 | 27 | 1.17 | 10.6 |

engineering [21, 22], can simulate the mechanical properties of failure of geological materials when the ultimate strength or yield limit is reached and can simulate a variety of structural forms, such as rock mass and soil. Moreover, it can also simulate artificial structures, such as support, anchor cable, and other geotechnical engineering mechanic problems. Through its embedded FISH language, users can write command flows to achieve more simulation functions, such as customizing the constitutive model, obtaining the stress and strain curves of a certain gridpoint, and extracting the data of a certain zone node. The distribution of elastic strain energy density of the surrounding rock in different areas of the roadway deduced above is realized by FISH language embedded in FLAC$^{3D}$, and subsequent analysis is carried out.

*4.1.2. Modeling.* The model takes the inclination as the $x$-axis, the strike direction as the $y$-axis, and the gravity direction as the $z$-axis. The lengths along the $x$, $y$, and $z$ axes are 50 m, 40 m, and 50 m, respectively. The cross-section width of the roadway is 4.2 m, and the middle line height is 2.65 m. The principle of grid division is that the area near the roadway is dense and the distance is sparse. Considering the influence range of the rock strata, the upper and lower strata are simplified, and the mechanical parameters of each layer are shown in Table 1. The model has a total of 40,116 nodes and 35,080 units. The model and the conditions of each rock layer are shown in Figure 4.

*4.1.3. Initial Stress.* Before the excavation of the roadway, the rock mass is in the in situ stress that has not been disturbed by the engineering, which is also called the initial stress. From the measured in situ stress, it can be seen that the initial stress field should not be underestimated to the underground engineering and is the source of deformation and failure to the rock mass surrounding the roadway. Meanwhile, the roadway excavation will produce disturbance to the initial stress field, which will redistribute the initial stress and produce high stress several times higher than the initial stress, so the simulation is combined with the initial stress field on site. According to the in situ stress test report, vertical stress is 10.34 MPa and the lateral pressure coefficient is 1.2.

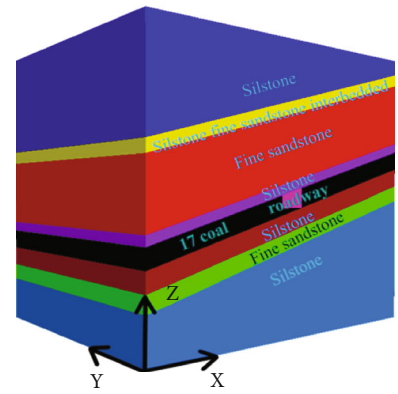


Figure 4: 3D mode diagram.

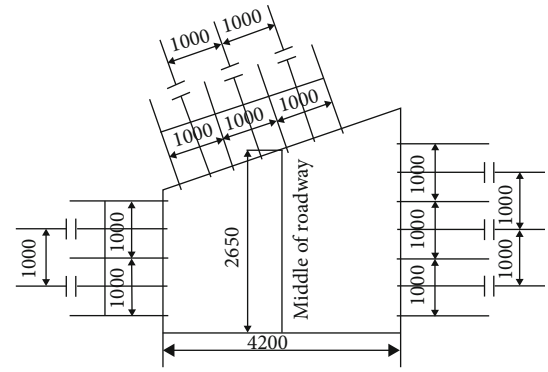


Figure 5: Combined support.

*4.1.4. Boundary Conditions.* The simulation uses the Mohr-Coulomb model to impose constraints on the boundaries by controlling the displacement. Vertical constraints are applied to the bottom of the model, horizontal constraints are applied to the left and right boundaries, and the top of the model is a free surface without any constraints. In addition, stress boundary conditions are applied according to the in situ stress.

*4.2. Supporting Scheme.* According to the parameters of the existing roadway section, the no support, original support, and combined support models are established, respectively. The combined support is shown in Figure 5. The roof adopts

Table 2: Mechanical parameters of bolt (anchor cable) anchorage.

| Supporting artifacts | Diameter (mm) | Length (mm) | Elasticity modulus (GPa) | Tensile strength (MPa) | Pretightening force (kN) |
|---|---|---|---|---|---|
| Anchor cables | 21.6 | 10000 | 200 | 200 | 60 |
| Bolts | 22 | 2500 | 190 | 250 | 80 |

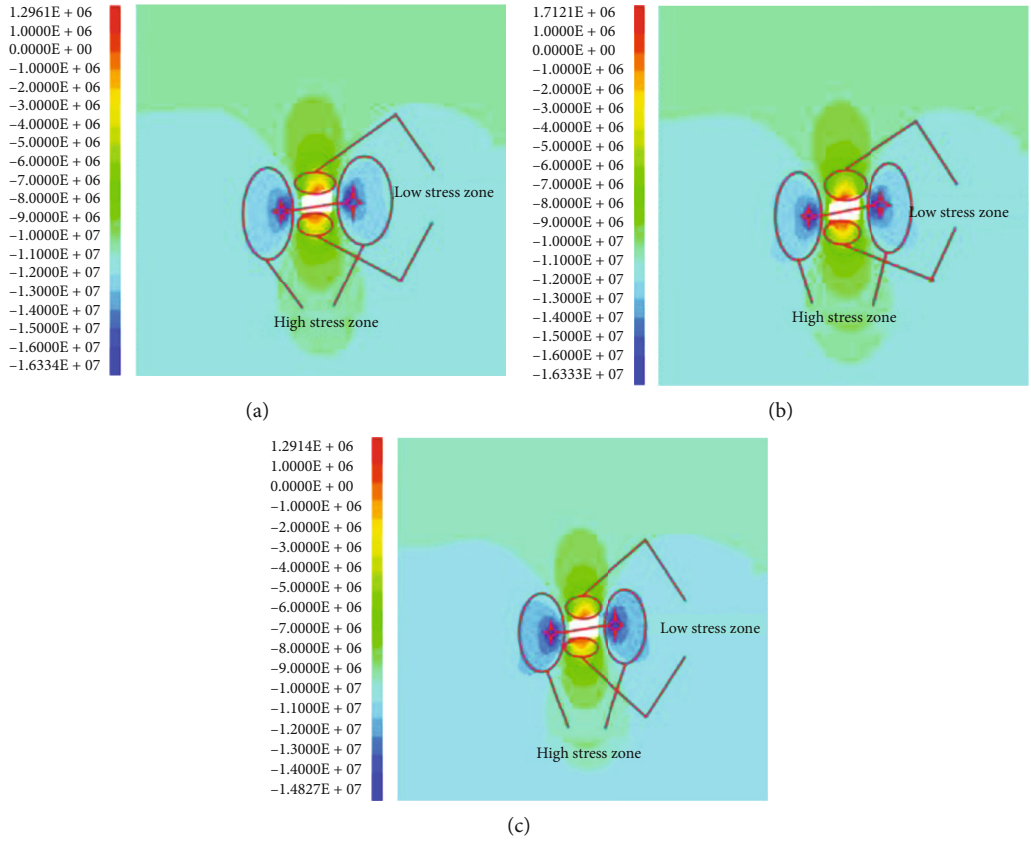


Figure 6: Vertical stress nephogram under different support methods. (a) No support. (b) Original support. (c) Combined support.

the combined support scheme of anchor mesh belt and anchor cable beam. The roof bolt uses $\Phi$22mm × 2500 mm high-strength bolt, the row distance between the bolts is 1000 mm × 1000 mm, the size of the roof anchor cable is $\Phi$ 21.6 mm × 10000 mm, and the row distance is 1000 mm × 1200 mm. The wall is supported by the anchor mesh belt. The bolt is $\Phi$22mm × 2500 mm type high-strength bolt, the row distance between bolts is 1000 mm × 1000 mm, the cable size is $\Phi$21.6 mm × 10000 mm, and the row distance is 1000 mm × 1200 mm. Cable element is adopted in bolt (anchor cable) in FLAC$^{3D}$, and mechanical parameters of bolt (cable) are shown in Table 2.

*4.3. Stress Distribution Law.* In order to eliminate the interference of the boundary, the vertical stress distribution of the surrounding rock of the roadway at $y = 20$ m is selected. The distribution of vertical stress under different support methods is shown in Figure 6.

It can be seen from Figure 6 that after the roadway excavation, high stress concentration zones appear on the two ribs of the roadway, and the direction of the connection between the two stress concentration zones is consistent with the coal seam tendency. The roof and floor of the roadway are all low-stress zones, and the floor has a small-scale tensile stress zone. This is because the roof and floor will release pressure and transfer to the two ribs after the excavation of the roadway, resulting in stress concentration on the two ribs. With the increase of the distance from the center of roadway, the vertical stress tends to be stable and close to the in situ rock stress. Overall, the vertical stress above the roof is slightly less than other positions. By comparing the vertical stress field under three different support methods, from no support to combined support, it can be seen that the high-stress areas on the two ribs of the roadway are obviously shrinking, the change of the roof is small, and the stress concentration area at the floor corner of the floor is significantly reduced. The vertical stress concentration range of the surrounding rock of the roadway is significantly decreased after the support, the combined support effect is better, and the vertical stress distribution is more uniform, indicating that the combined support is more conducive to the stability of the roadway.

In order to study the variation of the vertical stress around the roadway, starting from the roadway boundary,

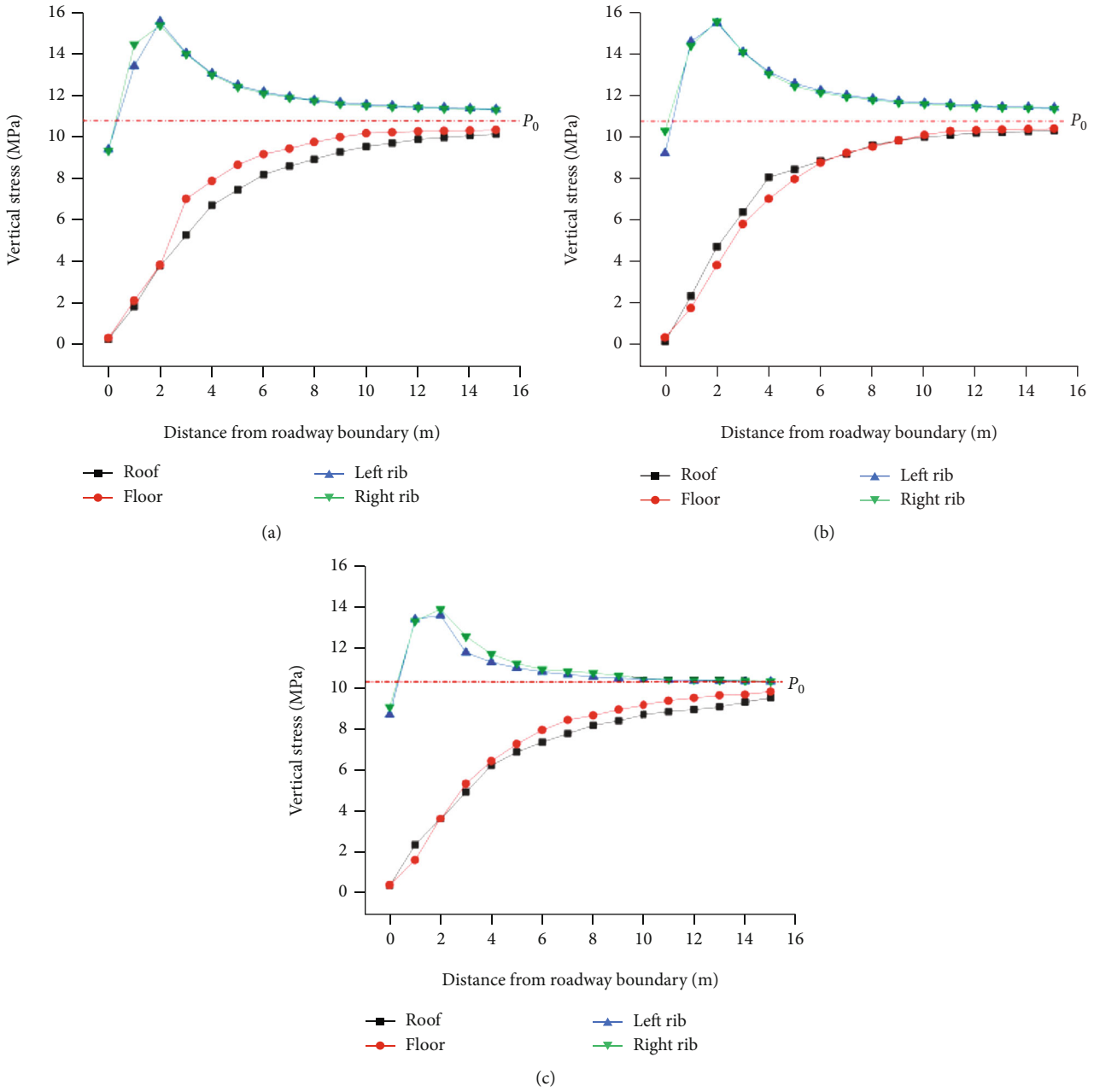


Figure 7: Vertical stress change curve under different support methods. (a) No support. (b) Original support. (c) Combined support.

measuring points are arranged within 15 m perpendicular to the roof, floor, and left and right ribs of the roadway, and the vertical stress values are recorded every 1 m. The vertical stress changes of the roof, floor, and right rib under different support methods are shown in Figure 7.

It can be seen from Figure 7 that the variation trend of vertical stress under different support methods is basically the same. The variation trend of vertical stress of the two ribs increases first and then decreases, gradually tends to be stable, close to the in situ rock stress. The vertical stress variation trend of the roof and floor is always increasing and finally tends to a stable value, which is close to the in situ rock stress. As can be seen from Figure 7(a), in the absence of support, the vertical stresses on the left and right ribs reach the maximum values of 15.55 MPa and 15.44 MPa at 2 m, respectively. In the range of 2~5 m, the vertical stress drops rapidly. After 5 m, the descending speed slows down and the vertical stress basically tends to be stable at 9 m, remaining at 11.3 MPa. The vertical stress grows rapidly in the range of 0 to 5 m in the roof and floor; in the range of 5 to 9 m, the growth rate becomes slower; at 9 m, it basically remains stable at 11.4 MPa and 11.37 MPa, respectively.

It can be seen from Figure 7(b) that under the original support condition, the vertical stresses on the left and right ribs reach the maximum of 15.42 MPa and 15.37 MPa at 2 m, which are slightly smaller than those without support. In the range of 2~5 m, the vertical stress drops rapidly. After 5 m, the descending speed becomes slower, and the vertical

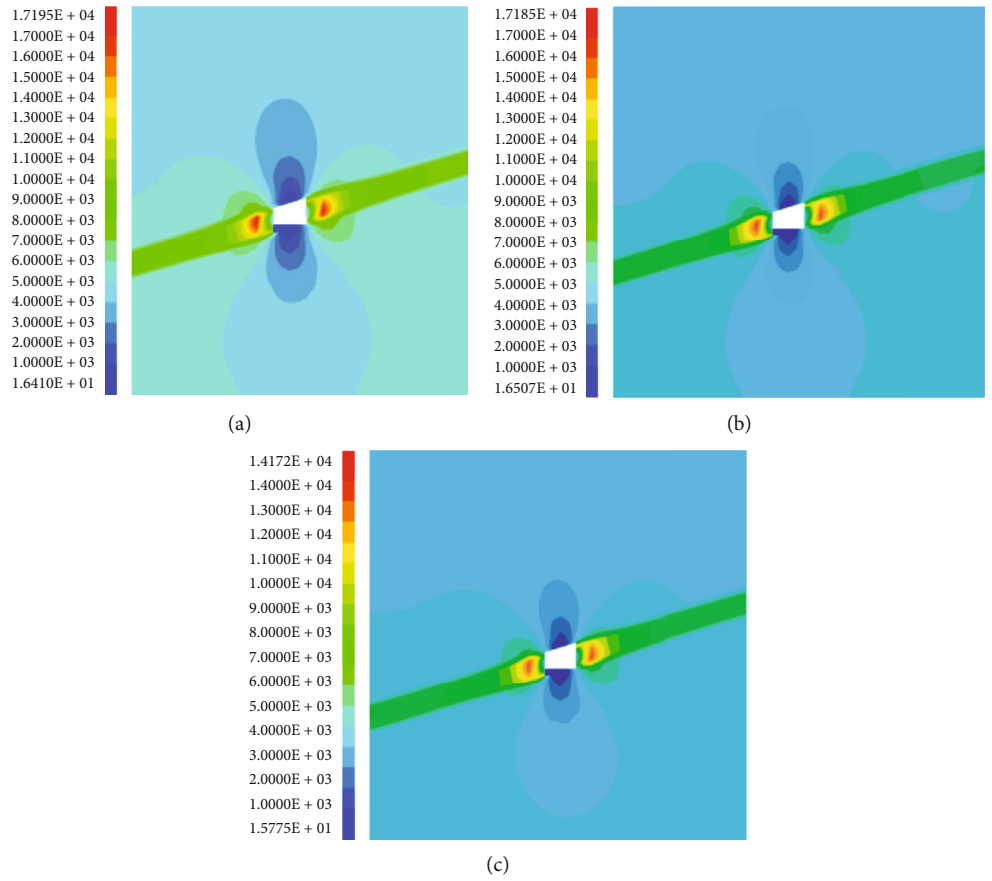


Figure 8: Energy density distribution nephogram of the three scheme. (a) No support. (b) Original support. (c) Combined support.

stress basically tends to be stable at 8 m, remaining at 11.3 MPa. The roof and the floor show a large difference in the range of 0 to 5 m. The vertical stress in the roof grows faster relative to the floor; in the range of 5 to 9 m, the growth rate becomes slower; at 9 m, it basically remains stable at 10.24 MPa and 10.15 MPa, respectively.

From Figure 7(c), it can be seen that the stress difference between the left and right ribs decreases significantly, and the change trend becomes significantly slower, which means that the stress concentration degree decreases significantly, and the stress peaks are 13.94 MPa and 13.88 MPa, respectively. The variation trend of the roof and the floor is basically the same and finally close to the in situ rock stress.

*4.4. Law of Energy Distribution.* Figure 8 shows the nephogram of energy distribution under different support methods, from which it can be seen that the overall energy of the coal seam is high, and a high energy zone appears at the position of about 2 m to the left and right of the roadway, which corresponds to the vertical stress high stress area. The energy of the roof and floor of the roadway is the smallest, extending 5 m up and down, respectively, to the low energy area. The rest of the locations have uniform energy distribution, and the overall energy of the lower part is greater than that of the upper part. This is because after the excavation of the roadway, the stress of the surrounding rock is redistributed. The elastic strain energy is concentrated near the surrounding rock of the roadway for the fine adjustment and tiny movement of a large number of surrounding rock particles. The energy at the position of the two ribs of the roadway and the junction of the floor and the two ribs is the largest, and the elastic deformation energy stored in the floor surrounding rock is the least, and the energy reduction is the largest. It means that after excavation, the floor of the roadway has been released and the stored energy has been reduced, and most of the elastic deformation energy has been turned into plastic dissipation energy, which is gradually reduced along the radial direction, corresponding to the vertical stress distribution. Comparing the energy density distribution nephogram under different support methods, it can be found that the range of high energy density in both ribs of the roadway after support has been reduced, and the low energy density area in the roof and the floor has been reduced and distributed more evenly.

Figure 9 shows the change curve of energy density under different supports. As can be seen from Figure 9(a), the overall variation trend of energy density is consistent with that of the vertical stress. The left and right ribs reach the maximum at 2 m, which are 15895.8 J/m$^3$ and 15637.4 J/m$^3$, respectively. In the range from 2 to 7 m, the energy density decreases rapidly. After 7 m from the roadway boundary, the energy density decreases slowly and gradually stabilizes,

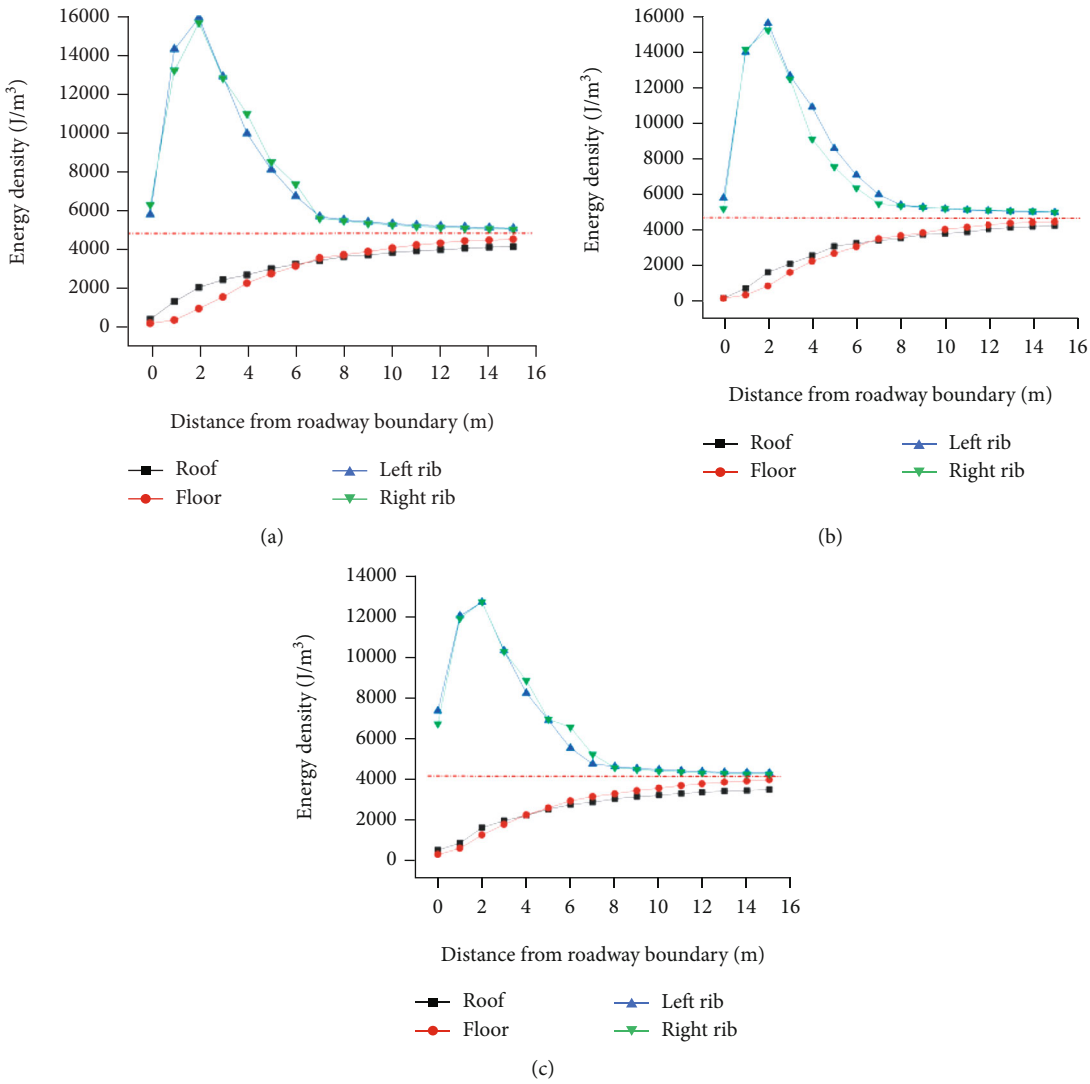


Figure 9: Energy density change curve under different support methods. (a) No support. (b) Original support. (c) Combined support.

basically remaining at about 4490 J/m$^3$. The roof and floor show a fast and then slow growth trend, and gradually stabilize after 7 m from the roadway boundary, and finally remain at about 4490 J/m$^3$. As can be seen from Figure 9(b), the left and right ribs reach the maximum at 2 m, which are 15679 J/m$^3$ and 15479 J/m$^3$, respectively. In the range of 2~7 m, the energy density of the left and right ribs varies, and the right rib is slightly smaller than the left rib, which is due to the support role to resist part of the deformation. After 7 m from the roadway boundary, the energy density decreases slowly and gradually stabilizes, basically keeping at about 4485 J/m$^3$. Compared with the condition without support, the growth trend of roof and floor is more uniform, and the energy density finally stays around 4485 J/m$^3$. It can be seen from Figure 9(c) that under the combined support condition, the peak energies of the left and right ribs are 12617 J/m$^3$ and 12632 J/m$^3$ respectively, which is lower than the first two cases and the overall energy difference is small. The energy density of the roof and floor is basically the same, and the energy of the floor is slightly larger than that of the roof.

## 5. Engineering Application Effect

Three roadway surface displacement stations are arranged in the original support and combined support roadway. The measuring stations are arranged by the "cross" point layout method, and the distance between the stations is 30~50 m. The data are further organized to get the amount of roof subsidence, floor heave, and right rib offset at the location of each measurement station and to compare and analyze the deformation of the original support and combined support of the roadway.

According to the monitoring data, the roadway surface displacement curves of the original support and the combined support were obtained through further processing and analysis. The roof subsidence, floor heave, and right rib offset of the roadway in different stages were compared, and the most representative group of curves was selected as shown in Figure 10.

From the roadway roof subsidence curve in Figure 10(a), it can be seen that the maximum roof subsidence of the floor heave in the original supporting roadway is about 247 mm, and the trend of continuous increase is obvious. The

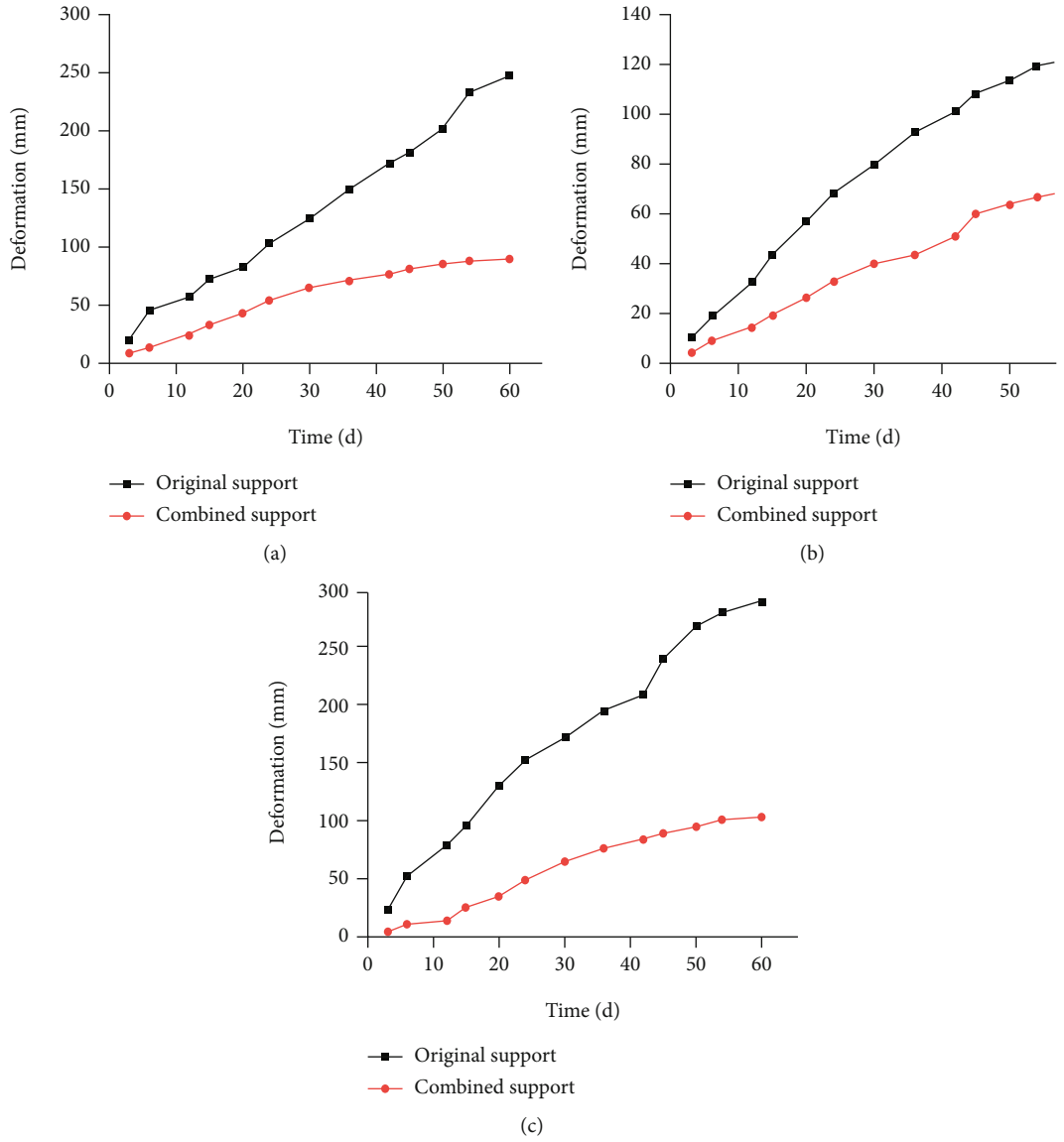


Figure 10: Roadway surface deformation curve. (a) Roof Subsidence. (b) Floor Heave. (c) Right Side Offset.

maximum roof subsidence in the combined support is about 90 mm, and the deformation is decreased by 63.56%, and the curve gradually stabilizes. From Figure 10(b), it can be seen that the floor heave maximum of the original support roadway is about 120 mm, the curve does not slow down, and the roadway floor heave will continue to increase. The floor heave maximum of roadway with combined support is 68 mm, and the deformation is reduced by 43.33%. Moreover, the curve starts to slow down when the monitoring time is about 45d, and the floor heave of the roadway gradually tends to be stable. As shown from Figure 10(c), the right rib offset maximum of the original supporting roadway is about 292 mm, which obviously shows a trend of continuous increase. The maximum right rib offset of the combined support roadway is about 104 mm, and the deformation is decreased by 64.38% and gradually tends to be stable. Through the above comparative analysis, it is obvious that after the roadway adopts the combined support technology, the roadway surrounding rock deformation is controlled, the overall stability of the roadway surrounding rock is improved, and the application effect of the technology is remarkable.

## 6. Conclusion

Based on the existing support parameters of Dongrong No. 2 Mine, this paper makes a comparative analysis of vertical stress and energy distribution under three support modes: no support, original support, and combined support and draws the following conclusions:

(1) After roadway excavation, the two sides of roadway are high stress areas, and the line direction is consistent with the tendency of coal seam. The roof and floor of the roadway are both low stress areas, and the floor appears in a small range of tensile stress area

(2) The variation trend of vertical stress under different support methods is consistent, and the variation trend of vertical stress on both ribs increases first and then decreases, gradually approaching the in situ rock stress. The vertical stress of roof and floor increases all the time and finally approaches the in situ rock stress. From no support to combined support, the area of high stress on both ribs of roadway is obviously reduced, the change of roof is small, and the stress concentration area of floor corner is obviously reduced. The vertical stress concentration range of roadway surrounding rock is obviously decreased after the support, and the combined support is more effective, and the vertical stress distribution is more uniform

(3) After the roadway excavation, the overall energy of the coal seam is high, and a high energy zone appears at about 2 m of the roadway, corresponding to the high vertical stress zone. The energy of the roof and floor of the roadway is the smallest, extending 5 m upward and downward to the low energy area. The rest of the positions have uniform energy distribution, and the overall energy of the lower part is larger than that of the upper part

(4) The variation trend of energy under different support methods is consistent with that of vertical stress. The variation trend of energy on both ribs increases first and then decreases. The variation trend of energy in the roof and floor is always increasing and finally tends to be stable. From no support to combined support, the high energy zone on both ribs of the roadway is obviously reduced. The energy concentration range of the roadway surrounding rock decreases after the support, the combined support effect is better, and the energy distribution is more uniform

(5) After the roadway adopts the combined support technology, the roof, floor, and right rib deformations are reduced by 63.56%, 43.33%, and 64.38%, respectively. The deformation of surrounding rock is controlled, and the overall stability of the surrounding rock is improved

## Data Availability

The rock mechanical parameters in this paper are all measured in the laboratory, and the status quo of roadway support and on-site monitoring data are all obtained through on-site investigation.

## Conflicts of Interest

The authors declare that they have no conflicts of interest.

## Acknowledgments

The research presented in this paper has been supported by the Central Government for the Reform and Development of Local Universities (2020YQ13).

## References

[1] D. J. Liu, J. P. Zuo, H. Y. Liu, Z. J. Hong, J. H. Wen, and Y. Shi, "Development and present situation of support theory and technology in coal mine roadway in China," *Journal of Mining Science and Technology*, vol. 5, no. 1, pp. 22–33, 2020.

[2] G. M. Zhao, X. B. Zhang, C. Wang, and X. R. Meng, "Mechanical analysis and numerical simulation for deep and shallow bearing structures of soft and broken roadway surrounding rock," *Journal of China Coal Society*, vol. 41, no. 7, pp. 1632–1642, 2016.

[3] Q. B. Meng, L. H. Kong, L. J. Han et al., "Stability control technology for deep soft and broken composite roof in coal roadway," *Journal of China Coal Society*, vol. 42, no. 10, pp. 2554–2564, 2017.

[4] S. Mehmet, "Two-and three-dimensional stability analysis of underground storage caverns in soft rock (Cappadocia, Turkey) by finite element method," *Journal of Mountain Science*, vol. 19, no. 4, pp. 1182–1202, 2022.

[5] P. Xu, R. S. Yang, J. J. Zuo et al., "Research progress of the fundamental theory and technology of rock blasting," *International Journal of Minerals, Metallurgy and Materials*, vol. 29, no. 4, pp. 705–716, 2022.

[6] M. S. Gao, N. Zhang, L. N. Dou, K. Wang, and J. G. Kan, "Study of roadway support parameters subjected to rock burst based on energy balance theory," *Journal of China University of Mining and Technology*, vol. 36, no. 4, pp. 426–430, 2007.

[7] W. J. Ju, "Energy checking design method of roadway with rock-brust danger," *Coal Mining Technology*, vol. 16, no. 3, pp. 81–83, 2011.

[8] A. W. Wang, D. W. Fan, Y. S. Pan et al., "Determination of three-level energy absorbing support parameters in rock burst roadway based on energy calculation," *Coal Science and Technology*, vol. 49, no. 6, pp. 72–81, 2021.

[9] Y. S. Pan, Q. X. Qi, A. W. Wang et al., "The theory and technology of three-level support for coal mine rockburst roadway," *Journal of China Coal Society*, vol. 45, no. 5, pp. 1585–1594, 2020.

[10] W. L. Gong, D. Y. Zhu, J. Wang, M. C. He, and D. L. Wang, "Deformation and energy equation verification of NPR anchor cable support roadway based on model test," *Journal of Mining & Safety Engineering*, vol. 37, no. 5, pp. 918–927, 2020.

[11] R. L. Shan, H. Yang, H. Zhong, and Y. Tao, "Design of support parameters and energy constitutive model yielding anchor blot," *Journal of China University of Mining & Technology*, vol. 43, no. 2, pp. 241–247, 2014.

[12] J. K. Lin, Y. Zhang, and Y. Hao, "Reasonable coal pillar size supported by high strength energy-absorbing rock bolt," *Coal Engineering*, vol. 53, no. 3, pp. 40–45, 2021.

[13] Z. Q. Ma, C. M. Tao, Y. J. Zuo, G. Y. Wu, and P. Liu, "Supporting technology of roadways with thick and soft roof based on energy balance theory," *Journal of Mining & Safety Engineering*, vol. 35, no. 3, pp. 496–502, 2018.

[14] F. T. Wang, J. J. Shang, B. Zhao, Q. H. Cao, and T. C. Niu, "Strengthened anchor cable support mechanism and its parameter optimization design for roadway's dynamic pressure section," *Journal of China University of Mining & Technology*, vol. 51, no. 1, pp. 56–66, 2022.

[15] H. X. Chen, M. Y. Wang, C. Z. Qi, and J. Li, "Mechanism of energy adjustment and balance of rock masses near a deep circular tunnel," *Chinese Journal of Geotechnical Engineering*, vol. 42, no. 10, pp. 1849–1857, 2020.

[16] Z. Hao, L. F. Guo, X. D. Zhao, G. X. Chen, and G. H. Zhang, "Analysis of burst failure energy characteristics of mining roadway surrounding rock," *Journal of China Coal Society*, vol. 45, no. 12, pp. 3995–4005, 2020.

[17] H. Y. Shi, N. J. Ma, J. J. Shi, N. Li, and G. W. Tan, "Simulation study on energy evolution and release of surrounding rock in stope," *Coal Science and Technology*, vol. 48, no. 3, pp. 106–111, 2020.

[18] J. W. Zheng, W. J. Ju, Z. Zhang et al., "Equivalent section supporting theory and its applications," *Journal of China Coal Society*, vol. 45, no. 3, pp. 1036–1043, 2020.

[19] J. W. Zheng, W. J. Ju, X. D. Sun et al., "Differentiation response characteristic of roadway deformation and rock supporting analysis," *Journal of Mining and Strata Control Engineering*, vol. 3, no. 3, pp. 13–20, 2021.

[20] D. P. Ma, Y. J. Yang, J. S. Cao, and L. Y. Xing, "Optimization design of cross section shape of deep roadways based on characteristics of energy release," *Journal of Central South University (Science and Technology)*, vol. 46, no. 9, pp. 3354–3360, 2015.

[21] Y. M. Chen and H. L. Liu, "Development and implementation of Duncan-Chang constitutive model in FLAC$^{3D}$," *Rock and Soil Mechanics*, vol. 28, no. 10, pp. 2123–2127, 2007.

[22] M. Wang, Z. F. Song, D. J. Zheng, W. L. Shen, P. F. Gou, and S. J. Wei, "Development and application of rock energy dissipation model in FLAC$^{3D}$," *Journal of China Coal Society*, vol. 46, no. 8, pp. 2565–2573, 2021.